Feasibility of RF Ablation at the Larmor Frequency for RF Field Visualization

K. Shultz[1], P. Stang[1], J. Pauly[1], and G. Scott[1]
[1]Electrical Engineering, Stanford University, Stanford, CA, United States

Introduction: Radiofrequency ablation is an effective minimally invasive treatment for tumors. One primary source of difficulty is monitoring and controlling the ablation region. MR currently has a role in RF ablation due to its capability for temperature monitoring. RF ablation is typically performed at 480 kHz. If instead the ablation were to be performed at the Larmor frequency, then the MR capability for B1 field mapping could be used to directly visualize the RF fields created by the ablation currents. Visualizing the RF fields may enable better control of the ablation currents, enabling better control of lesion shape and size and improving repeatability. We demonstrate the feasibility of performing RF ablations at 64 MHz and show preliminary results from imaging the RF fields from the ablation.

Methods: 64 MHz Ablation System: The system used for the ablation is shown in Fig. 1. A Medusa console [1] was used to control the RF. The console provided an RF signal with variable amplitude to a power amplifier that was then transmitted to the ablation electrode. Voltage and current measurements were acquired from an inline voltage and current coupler and fed back to the receive port of the Medusa console. The impedance at the ablation electrode was calculated through an impedance transformation to account for the length of transmission line. Temperature data was acquired using an MR compatible fiber optic temperature sensor with a Luxtron m3300 Biomedical Lab Kit from LumaSense (Santa Clara, CA, USA). Real-time temperature and impedance measurements were provided to the operator through a GUI developed in Matlab (MathWorks, Natick, MA, USA). The operator controlled the ablation power with the GUI based on the impedance and temperature readings. An *ex-vivo* chicken sample was used for the ablation. The ablation electrode was bipolar, with two tines on each polarity (see Fig 2).

Imaging: Separate images were acquired using either the ablation electrode or the body coil as transmit elements. Field maps were acquired with the AFI B1 mapping sequence [3]. 3 different excitation magnitudes were used for the ablation electrode images due to the large dynamic range of B1 observed in the vicinity of the wires, and then the field maps combined. The images from the first TR of the AFI sequence were used as T1 weighted images. The sequence parameters were TR8.5ms, n=10, FOV=6.4cm, resolution=1mm^{2}x2mm, 20 slices.

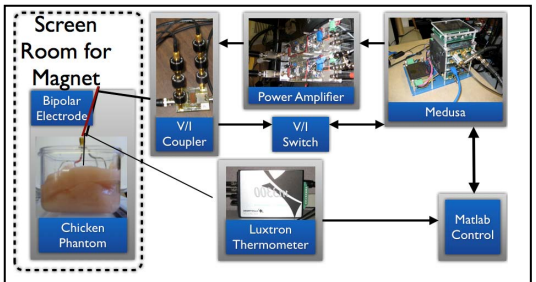

Figure 1: *Block diagram of ablation configuration. The operator controls the ablation power while observing live impedance and temperature readings to monitor the progress of the ablation.*

Figure 2: *Ablation electrode (left) and chicken before (center) and after (right) ablation. The region around the electrode is cooked while the edges remain raw.*

Results: The chicken sample was visibly cooked around the electrode (Fig 2). During the ablation, the impedance decreased as the temperature increased (Fig 3), due to the increasing conductivity of tissue with temperature. As the tissue becomes denatured, the impedance change levels off. The impedance measurement becomes noisier as the temperature increases, likely due to boiling and cavitation at the electrode interfering with the electrical contact.

The B1 maps taken with the ablation electrode (Fig 4) show a change in the field patterns and therefore the current patterns. Strong fields are expected around current carrying wires where the current density is most concentrated, with the field strength proportional to the current. The field maps show some change in the distribution of the current along the electrode during the ablation. The slice near the top of the phantom shows stronger fields along the horizontal wire leading to the exterior lead, while the slice lower in the phantom shows smaller fields around the interior leads. This likely indicates that the current has shifted to the exterior leads as the region between the interior leads becomes denatured and increases in impedance.

The T1 weighted images show a brightening in the ablated region (Fig 5) surrounded by a darkened region. The images acquired with the uniform B1 and with the electrode B1 show a similar changed region, but the electrode image shows a hypointense region around the ablation lesion surrounded by another brighter region, while the uniform B1 image shows only the central brightening and then darkening everywhere else. Further investigation is needed into the relation between these regions and the exact size of the lesion.

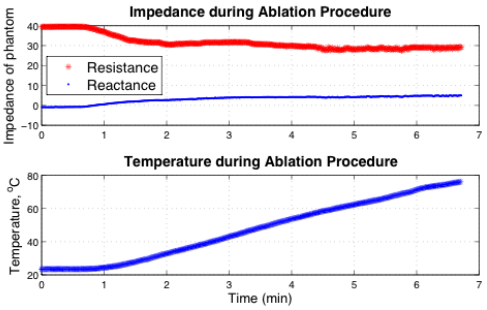

Figure 3: *Impedance and temperature measurements during ablation.*

Discussion: Field mapping of the ablation current shows clear changes in the current carried on each lead. It will be useful to gain more control with multi-tined and multi-polar ablation electrodes. With a multipolar electrode, power could be diverted to leads that have lower current to provide more even heating. It is theoretically possible to image the current density in the tissue [4] without rotating the subject [5], but the necessary SNR is difficult to achieve due to the low fields produced by the distributed current density and the overwhelming fields from the currents on the wires. This may be an avenue of future exploration.

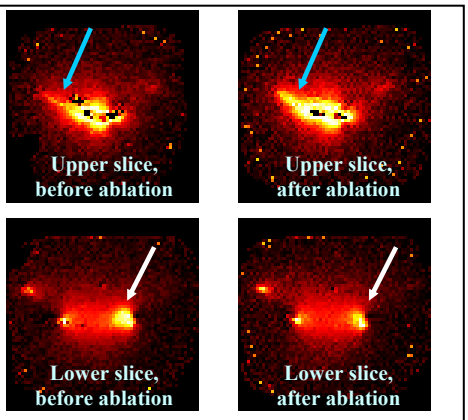

Figure 4: *B1 maps from the ablation current before (left) and after (right) the treatment for an upper (top) and lower (bottom) slice. Blue arrows indicate the horizontal wire at the top of the electrode, where currents became more concentrated after ablation. White arrows indicate the vertical wires lower in the phantom, where there is less current after ablation.*

Conclusions: We have demonstrated that RF ablation at 64 MHz is feasible. When the ablation is performed at the Larmor frequency, RF field mapping can provide new information about the location of the ablation currents. This has the potential to improve control of the ablation process.

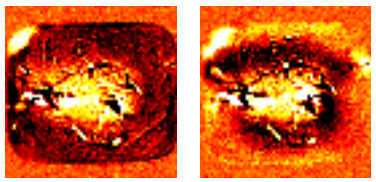

Figure 5: *Difference between pre-and post-ablation T1 weighted images with uniform B1 (left) and B1 from the ablation wires (right) for a lower slice. Both show brightening in the ablated region surrounded by a hypointense region.*

References:
[1] Stang et al, Proc. 15th ISMRM, p925, 2007. [2] Scott et al, Proc 17th ISMRM, p3025, 2009. [3] Yarnykh, MRM 57:292, 2007. [4] Scott et al, MRM. 28:186, 1992. [5] Shultz et al, Proc. 15th ISMRM, p1131, 2007.

Acknowledgement: This work partly supported by NIH R01 EB008108, NIH R21 EB007715, NIH R33 CA1182756.